Observation of $e^+e^- \to \omega\chi_{c1,2}$ near $\sqrt{s} = 4.42$ and 4.6 GeV

M. Ablikim,[1] M. N. Achasov,[9,e] X. C. Ai,[1] O. Albayrak,[5] M. Albrecht,[4] D. J. Ambrose,[44] A. Amoroso,[49a,49c] F. F. An,[1] Q. An,[46,a] J. Z. Bai,[1] R. Baldini Ferroli,[20a] Y. Ban,[31] D. W. Bennett,[19] J. V. Bennett,[5] M. Bertani,[20a] D. Bettoni,[21a] J. M. Bian,[43] F. Bianchi,[49a,49c] E. Boger,[23,c] I. Boyko,[23] R. A. Briere,[5] H. Cai,[51] X. Cai,[1,a] O. Cakir,[40a] A. Calcaterra,[20a] G. F. Cao,[1] S. A. Cetin,[40b] J. F. Chang,[1,a] G. Chelkov,[23,c,d] G. Chen,[1] H. S. Chen,[1] H. Y. Chen,[2] J. C. Chen,[1] M. L. Chen,[1,a] S. J. Chen,[29] X. Chen,[1,a] X. R. Chen,[26] Y. B. Chen,[1,a] H. P. Cheng,[17] X. K. Chu,[31] G. Cibinetto,[21a] H. L. Dai,[1,a] J. P. Dai,[34] A. Dbeyssi,[14] D. Dedovich,[23] Z. Y. Deng,[1] A. Denig,[22] I. Denysenko,[23] M. Destefanis,[49a,49c] F. De Mori,[49a,49c] Y. Ding,[27] C. Dong,[30] J. Dong,[1,a] L. Y. Dong,[1] M. Y. Dong,[1,a] Z. L. Dou,[29] S. X. Du,[53] P. F. Duan,[1] E. E. Eren,[40b] J. Z. Fan,[39] J. Fang,[1,a] S. S. Fang,[1] X. Fang,[46,a] Y. Fang,[1] R. Farinelli,[21a,21b] L. Fava,[49b,49c] O. Fedorov,[23] F. Feldbauer,[22] G. Felici,[20a] C. Q. Feng,[46,a] E. Fioravanti,[21a] M. Fritsch,[14,22] C. D. Fu,[1] Q. Gao,[1] X. L. Gao,[46,a] X. Y. Gao,[2] Y. Gao,[39] Z. Gao,[46,a] I. Garzia,[21a] K. Goetzen,[10] L. Gong,[30] W. X. Gong,[1,a] W. Gradl,[22] M. Greco,[49a,49c] M. H. Gu,[1,a] Y. T. Gu,[12] Y. H. Guan,[1] A. Q. Guo,[1] L. B. Guo,[28] Y. Guo,[1] Y. P. Guo,[22] Z. Haddadi,[25] A. Hafner,[22] S. Han,[51] X. Q. Hao,[15] F. A. Harris,[42] K. L. He,[1] T. Held,[4] Y. K. Heng,[1,a] Z. L. Hou,[1] C. Hu,[28] H. M. Hu,[1] J. F. Hu,[49a,49c] T. Hu,[1,a] Y. Hu,[1] G. S. Huang,[46,a] J. S. Huang,[15] X. T. Huang,[33] Y. Huang,[29] T. Hussain,[48] Q. Ji,[1] Q. P. Ji,[30] X. B. Ji,[1] X. L. Ji,[1,a] L. W. Jiang,[51] X. S. Jiang,[1,a] X. Y. Jiang,[30] J. B. Jiao,[33] Z. Jiao,[17] D. P. Jin,[1,a] S. Jin,[1] T. Johansson,[50] A. Julin,[43] N. Kalantar-Nayestanaki,[25] X. L. Kang,[1] X. S. Kang,[30] M. Kavatsyuk,[25] B. C. Ke,[5] P. Kiese,[22] R. Kliemt,[14] B. Kloss,[22] O. B. Kolcu,[40b,h] B. Kopf,[4] M. Kornicer,[42] W. Kuehn,[24] A. Kupsc,[50] J. S. Lange,[24,a] M. Lara,[19] P. Larin,[14] C. Leng,[49c] C. Li,[50] C. H. Li,[1] Cheng Li,[46,a] D. M. Li,[53] F. Li,[1,a] F. Y. Li,[31] G. Li,[1] H. B. Li,[1] J. C. Li,[1] Jin Li,[32] K. Li,[13] K. Li,[33] Lei Li,[3] P. R. Li,[41] Q. Y. Li,[33] T. Li,[33] W. D. Li,[1] W. G. Li,[1] X. L. Li,[33] X. M. Li,[12] X. N. Li,[1,a] X. Q. Li,[30] Z. B. Li,[38] H. Liang,[46,a] Y. F. Liang,[36] Y. T. Liang,[24] G. R. Liao,[11] D. X. Lin,[14] B. J. Liu,[1] C. X. Liu,[1] D. Liu,[46,a] F. H. Liu,[35] Fang Liu,[1] Feng Liu,[6] H. B. Liu,[12] H. H. Liu,[1] H. H. Liu,[16] H. M. Liu,[1] J. Liu,[1] J. B. Liu,[46,a] J. P. Liu,[51] J. Y. Liu,[1] K. Liu,[39] K. Y. Liu,[27] L. D. Liu,[31] P. L. Liu,[1,a] Q. Liu,[41] S. B. Liu,[46,a] X. Liu,[26] Y. B. Liu,[30] Z. A. Liu,[1,a] Zhiqing Liu,[22] H. Loehner,[25] X. C. Lou,[1,a,g] H. J. Lu,[17] J. G. Lu,[1,a] Y. Lu,[1] Y. P. Lu,[1,a] C. L. Luo,[28] M. X. Luo,[52] T. Luo,[42] X. L. Luo,[1,a] X. R. Lyu,[41] F. C. Ma,[27] H. L. Ma,[1] L. L. Ma,[33] Q. M. Ma,[1] T. Ma,[1] X. N. Ma,[30] X. Y. Ma,[1,a] Y. M. Ma,[33] F. E. Maas,[14] M. Maggiora,[49a,49c] Y. J. Mao,[31] Z. P. Mao,[1] S. Marcello,[49a,49c] J. G. Messchendorp,[25] J. Min,[1,a] R. E. Mitchell,[19] X. H. Mo,[1,a] Y. J. Mo,[6] C. Morales Morales,[14] N. Yu. Muchnoi,[9,e] H. Muramatsu,[43] Y. Nefedov,[23] F. Nerling,[14] I. B. Nikolaev,[9,e] Z. Ning,[1,a] S. Nisar,[8] S. L. Niu,[1,a] X. Y. Niu,[1] S. L. Olsen,[32] Q. Ouyang,[1,a] S. Pacetti,[20b] Y. Pan,[46,a] P. Patteri,[20a] M. Pelizaeus,[4] H. P. Peng,[46,a] K. Peters,[10] J. Pettersson,[50] J. L. Ping,[28] R. G. Ping,[1] R. Poling,[43] V. Prasad,[1] H. R. Qi,[2] M. Qi,[29] S. Qian,[1,a] C. F. Qiao,[41] L. Q. Qin,[33] N. Qin,[51] X. S. Qin,[1] Z. H. Qin,[1,a] J. F. Qiu,[1] K. H. Rashid,[48] C. F. Redmer,[22] M. Ripka,[22] G. Rong,[1] Ch. Rosner,[14] X. D. Ruan,[12] V. Santoro,[21a] A. Sarantsev,[23,f] M. Savrié,[21b] K. Schoenning,[50] S. Schumann,[22] W. Shan,[31] M. Shao,[46,a] C. P. Shen,[2] P. X. Shen,[30] X. Y. Shen,[1] H. Y. Sheng,[1] W. M. Song,[1] X. Y. Song,[1] S. Sosio,[49a,49c] S. Spataro,[49a,49c] G. X. Sun,[1] J. F. Sun,[15] S. S. Sun,[1] Y. J. Sun,[46,a] Y. Z. Sun,[1] Z. J. Sun,[1,a] Z. T. Sun,[19] C. J. Tang,[36] X. Tang,[1] I. Tapan,[40c] E. H. Thorndike,[44] M. Tiemens,[25] M. Ullrich,[24] I. Uman,[40d] G. S. Varner,[42] B. Wang,[30] B. L. Wang,[41] D. Wang,[31] D. Y. Wang,[31] K. Wang,[1,a] L. L. Wang,[1] L. S. Wang,[1] M. Wang,[33] P. Wang,[1] P. L. Wang,[1] S. G. Wang,[31] W. Wang,[1,a] W. P. Wang,[46,a] X. F. Wang,[39] Y. D. Wang,[14] Y. F. Wang,[1,a] Y. Q. Wang,[22] Z. Wang,[1,a] Z. G. Wang,[1,a] Z. H. Wang,[46,a] Z. Y. Wang,[1] T. Weber,[22] D. H. Wei,[11] J. B. Wei,[31] P. Weidenkaff,[22] S. P. Wen,[1] U. Wiedner,[4] M. Wolke,[50] L. H. Wu,[1] Z. Wu,[1,a] L. Xia,[46,a] L. G. Xia,[39] Y. Xia,[18] D. Xiao,[1] H. Xiao,[47] Z. J. Xiao,[28] Y. G. Xie,[1,a] Q. L. Xiu,[1,a] G. F. Xu,[1] L. Xu,[1] Q. J. Xu,[13] Q. N. Xu,[41] X. P. Xu,[37] L. Yan,[49a,49c] W. B. Yan,[46,a] W. C. Yan,[46,a] Y. H. Yan,[18] H. J. Yang,[34] H. X. Yang,[1] L. Yang,[51] Y. X. Yang,[11] M. Ye,[1,a] M. H. Ye,[7] J. H. Yin,[1] B. X. Yu,[1,a] C. X. Yu,[30] J. S. Yu,[26] C. Z. Yuan,[1] W. L. Yuan,[29] Y. Yuan,[1] A. Yuncu,[40b,b] A. A. Zafar,[48] A. Zallo,[20a] Y. Zeng,[18] Z. Zeng,[46,a] B. X. Zhang,[1] B. Y. Zhang,[1,a] C. Zhang,[29] C. C. Zhang,[1] D. H. Zhang,[1] H. H. Zhang,[38] H. Y. Zhang,[1,a] J. J. Zhang,[1] J. L. Zhang,[1] J. Q. Zhang,[1] J. W. Zhang,[1,a] J. Y. Zhang,[1] J. Z. Zhang,[1] K. Zhang,[1] L. Zhang,[1] X. Y. Zhang,[33] Y. Zhang,[1] Y. H. Zhang,[1,a] Y. N. Zhang,[41] Y. T. Zhang,[46,a] Yu Zhang,[41] Z. H. Zhang,[6] Z. P. Zhang,[46] Z. Y. Zhang,[51] G. Zhao,[1] J. W. Zhao,[1,a] J. Y. Zhao,[1] J. Z. Zhao,[1,a] Lei Zhao,[46,a] Ling Zhao,[1] M. G. Zhao,[30] Q. Zhao,[1] Q. W. Zhao,[1] S. J. Zhao,[53] T. C. Zhao,[1] Y. B. Zhao,[1,a] Z. G. Zhao,[46,a] A. Zhemchugov,[23,c] B. Zheng,[47] J. P. Zheng,[1,a] W. J. Zheng,[33] Y. H. Zheng,[41] B. Zhong,[28] L. Zhou,[1,a] X. Zhou,[51] X. K. Zhou,[46,a] X. R. Zhou,[46,a] X. Y. Zhou,[1] K. Zhu,[1] K. J. Zhu,[1,a] S. Zhu,[1] S. H. Zhu,[45] X. L. Zhu,[39] Y. C. Zhu,[46,a] Y. S. Zhu,[1] Z. A. Zhu,[1] J. Zhuang,[1,a] L. Zotti,[49a,49c] B. S. Zou,[1] and J. H. Zou[1]

(BESIII Collaboration)

[1]*Institute of High Energy Physics, Beijing 100049, People's Republic of China*
[2]*Beihang University, Beijing 100191, People's Republic of China*

[3]*Beijing Institute of Petrochemical Technology, Beijing 102617, People's Republic of China*
[4]*Bochum Ruhr-University, D-44780 Bochum, Germany*
[5]*Carnegie Mellon University, Pittsburgh, Pennsylvania 15213, USA*
[6]*Central China Normal University, Wuhan 430079, People's Republic of China*
[7]*China Center of Advanced Science and Technology,*
Beijing 100190, People's Republic of China
[8]*COMSATS Institute of Information Technology, Lahore, Defence Road,*
Off Raiwind Road, 54000 Lahore, Pakistan
[9]*G.I. Budker Institute of Nuclear Physics SB RAS (BINP), Novosibirsk 630090, Russia*
[10]*GSI Helmholtzcentre for Heavy Ion Research GmbH, D-64291 Darmstadt, Germany*
[11]*Guangxi Normal University, Guilin 541004, People's Republic of China*
[12]*GuangXi University, Nanning 530004, People's Republic of China*
[13]*Hangzhou Normal University, Hangzhou 310036, People's Republic of China*
[14]*Helmholtz Institute Mainz, Johann-Joachim-Becher-Weg 45, D-55099 Mainz, Germany*
[15]*Henan Normal University, Xinxiang 453007, People's Republic of China*
[16]*Henan University of Science and Technology, Luoyang 471003, People's Republic of China*
[17]*Huangshan College, Huangshan 245000, People's Republic of China*
[18]*Hunan University, Changsha 410082, People's Republic of China*
[19]*Indiana University, Bloomington, Indiana 47405, USA*
[20a]*INFN Laboratori Nazionali di Frascati, I-00044 Frascati, Italy;*
[20b]*INFN and University of Perugia, I-06100 Perugia, Italy*
[21a]*INFN Sezione di Ferrara, I-44122 Ferrara, Italy*
[21b]*University of Ferrara, I-44122 Ferrara, Italy*
[22]*Johannes Gutenberg University of Mainz, Johann-Joachim-Becher-Weg 45,*
D-55099 Mainz, Germany
[23]*Joint Institute for Nuclear Research, 141980 Dubna, Moscow region, Russia*
[24]*Justus Liebig University Giessen, II. Physikalisches Institut, Heinrich-Buff-Ring 16,*
D-35392 Giessen, Germany
[25]*KVI-CART, University of Groningen, NL-9747 AA Groningen, Netherlands*
[26]*Lanzhou University, Lanzhou 730000, People's Republic of China*
[27]*Liaoning University, Shenyang 110036, People's Republic of China*
[28]*Nanjing Normal University, Nanjing 210023, People's Republic of China*
[29]*Nanjing University, Nanjing 210093, People's Republic of China*
[30]*Nankai University, Tianjin 300071, People's Republic of China*
[31]*Peking University, Beijing 100871, People's Republic of China*
[32]*Seoul National University, Seoul, 151-747 Korea*
[33]*Shandong University, Jinan 250100, People's Republic of China*
[34]*Shanghai Jiao Tong University, Shanghai 200240, People's Republic of China*
[35]*Shanxi University, Taiyuan 030006, People's Republic of China*
[36]*Sichuan University, Chengdu 610064, People's Republic of China*
[37]*Soochow University, Suzhou 215006, People's Republic of China*
[38]*Sun Yat-Sen University, Guangzhou 510275, People's Republic of China*
[39]*Tsinghua University, Beijing 100084, People's Republic of China*
[40a]*Ankara University, 06100 Tandogan, Ankara, Turkey*
[40b]*Istanbul Bilgi University, 34060 Eyup, Istanbul, Turkey*
[40c]*Uludag University, 16059 Bursa, Turkey*
[40d]*Near East University, Nicosia, North Cyprus, Mersin 10, Turkey*
[41]*University of Chinese Academy of Sciences, Beijing 100049, People's Republic of China*
[42]*University of Hawaii, Honolulu, Hawaii 96822, USA*
[43]*University of Minnesota, Minneapolis, Minnesota 55455, USA*
[44]*University of Rochester, Rochester, New York 14627, USA*
[45]*University of Science and Technology Liaoning, Anshan 114051, People's Republic of China*
[46]*University of Science and Technology of China, Hefei 230026, People's Republic of China*
[47]*University of South China, Hengyang 421001, People's Republic of China*
[48]*University of the Punjab, Lahore-54590, Pakistan*
[49a]*University of Turin, I-10125 Turin, Italy*
[49b]*University of Eastern Piedmont, I-15121 Alessandria, Italy*
[49c]*INFN, I-10125 Turin, Italy*
[50]*Uppsala University, Box 516, SE-75120 Uppsala, Sweden*
[51]*Wuhan University, Wuhan 430072, People's Republic of China*

^{52}*Zhejiang University, Hangzhou 310027, People's Republic of China*
^{53}*Zhengzhou University, Zhengzhou 450001, People's Republic of China*

Based on data samples collected with the BESIII detector operating at the BEPCII storage ring at center-of-mass energies $\sqrt{s} > 4.4$ GeV, the processes $e^+e^- \to \omega\chi_{c1,2}$ are observed for the first time. With an integrated luminosity of 1074 pb^{-1} near $\sqrt{s} = 4.42$ GeV, a significant $\omega\chi_{c2}$ signal is found, and the cross section is measured to be $(20.9 \pm 3.2 \pm 2.5)$ pb. With 567 pb^{-1} near $\sqrt{s} = 4.6$ GeV, a clear $\omega\chi_{c1}$ signal is seen, and the cross section is measured to be $(9.5 \pm 2.1 \pm 1.3)$ pb, while evidence is found for an $\omega\chi_{c2}$ signal. The first errors are statistical, and the second are systematic. Due to low luminosity or low cross section at other energies, no significant signals are observed. In the $\omega\chi_{c2}$ cross section, an enhancement is seen around $\sqrt{s} = 4.42$ GeV. Fitting the cross section with a coherent sum of the $\psi(4415)$ Breit-Wigner function and a phase-space term, the branching fraction $\mathcal{B}(\psi(4415) \to \omega\chi_{c2})$ is obtained to be of the order of 10^{-3}.

In recent years, charmonium physics gained renewed strong interest from both the theoretical and the experimental side, due to the observation of charmoniumlike states, such as $X(3872)$ [1,2], $Y(4260)$ [3–5], $Y(4360)$ [6,7], and $Y(4660)$ [7]. These states do not fit in the conventional charmonium spectroscopy and could be exotic states that lie outside the quark model [8]. Moreover, charged charmoniumlike states $Z_c(3900)$ [9–12], $Z_c(3885)$ [13,14], $Z_c(4020)$ [15,16], and $Z_c(4025)$ [17,18] or their neutral partners were observed, which might indicate the presence of new dynamics in this energy region. Searches for new decay modes and measurements of their line shapes may help us gain a better understanding of the nature of charmonium(like) states.

Most recently, BESIII has observed the process $e^+e^- \to \omega\chi_{c0}$ around $\sqrt{s} = 4.23$ GeV [19], which has first been proposed in Ref. [20]. As the line shape is incompatible with that of $Y(4260)$ in $e^+e^- \to \pi^+\pi^- J/\psi$, the authors of Ref. [21] suggest the excess of $\omega\chi_{c0}$ events due to a missing charmonium state, while Ref. [22] attributes it to the tail of the $\psi(4160)$. A similar pattern could be expected for the other spin triplet P-wave states $\chi_{c1,2}$. It is therefore very interesting to search for $e^+e^- \to \omega\chi_{c0,1,2}$ in the BESIII data collected at $\sqrt{s} > 4.4$ GeV. The ω transition may help us to establish connections between these charmonium(like) states.

In this paper, we report on a study of $e^+e^- \to \omega\chi_{cJ}(J = 0, 1, 2)$ based on the e^+e^- annihilation data collected with the BESIII detector [23] at five energy points in the range $4.416 \le \sqrt{s} \le 4.599$ GeV. The integrated luminosity of

this data is measured by using Bhabha scattering with an accuracy of 1.0% [24], and the center-of-mass energies are measured by using the dimuon process [25]. The $\chi_{c1,2}$ states are detected via $\chi_{c1,2} \to \gamma J/\psi$, $J/\psi \to \ell^+\ell^-(\ell = e, \mu)$, and the ω is reconstructed via the $\omega \to \pi^+\pi^-\pi^0$ decay mode. For $e^+e^- \to \omega\chi_{c0}$, χ_{c0} is reconstructed via its decays to $\pi^+\pi^-$ or K^+K^-.

Since the final state of the process $e^+e^- \to \omega\chi_{c1,2}$ is $\gamma\pi^+\pi^-\pi^0\ell^+\ell^-$, signal candidates must have exactly four tracks with zero net charge, a π^0 candidate, and a photon. The event selection criteria are the same as described in Ref. [19]. A five constraint (5C)-kinematic fit is performed constraining the total four momentum of the final state to the initial four momentum of the colliding beams, and the invariant mass of the two photons from π^0 is constrained to the nominal π^0 mass. The χ^2_{5C} of candidate events is required to be less than 60. The scatter plots of $M(\ell^+\ell^-)$ versus $M(\pi^+\pi^-\pi^0)$ after the above requirements are shown in Figs. 1(a) and 1(c) for data at $\sqrt{s} = 4.416$ GeV and 4.599 GeV. Clear signals are seen in the ω and J/ψ signal regions, which are defined as $0.75 \le M(\pi^+\pi^-\pi^0) \le 0.81$ GeV/c^2 for ω and $3.08 \le M(\ell^+\ell^-) \le 3.12$ GeV/c^2 for J/ψ, respectively. The mass resolution for J/ψ is found to be 8 MeV/c^2 in Monte Carlo (MC) simulations. The scatter plots of $M(\pi^+\pi^-\pi^0)$ versus $M(\gamma\ell^+\ell^-)$ after the J/ψ requirement are shown in Figs. 1(b) and 1(d). The signal regions of χ_{c1} and χ_{c2} are set to be [3.49, 3.53] and [3.54, 3.58] GeV/c^2, respectively, and the region [3.39, 3.47] GeV/c^2 is taken as the $\chi_{c1,2}$ sideband. Clear accumulations of events can be seen in the χ_{c2} signal region

^{a}Also at State Key Laboratory of Particle Detection and Electronics, Beijing 100049, Hefei 230026, People's Republic of China.
^{b}Also at Bogazici University, 34342 Istanbul, Turkey.
^{c}Also at the Moscow Institute of Physics and Technology, Moscow 141700, Russia.
^{d}Also at the Functional Electronics Laboratory, Tomsk State University, Tomsk 634050, Russia.
^{e}Also at the Novosibirsk State University, Novosibirsk 630090, Russia.
^{f}Also at the NRC "Kurchatov Institute", PNPI, 188300 Gatchina, Russia.
^{g}Also at University of Texas at Dallas, Richardson, Texas 75083, USA.
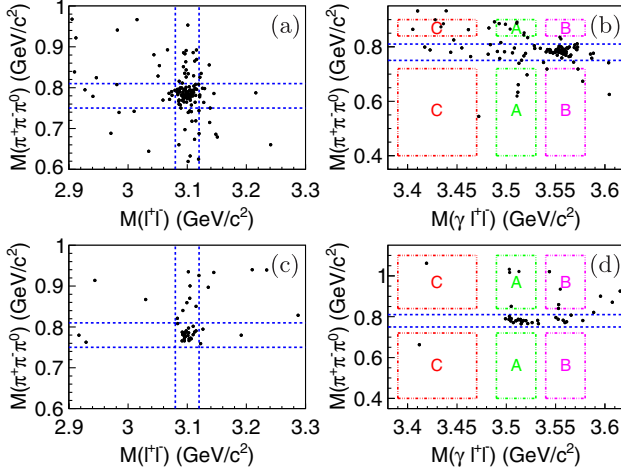^{h}Also at Istanbul Arel University, 34295 Istanbul, Turkey.

FIG. 1. Scatter plots for data at $\sqrt{s} = 4.416$ GeV [(a) and (b)] and 4.599 GeV [(c) and (d)]. Plots (a) and (c) are $M(\ell^+\ell^-)$ versus $M(\pi^+\pi^-\pi^0)$, the blue dashed lines mark the signal region of ω or J/ψ. Plots (b) and (d) are $M(\pi^+\pi^-\pi^0)$ versus $M(\gamma\ell^+\ell^-)$, the blue dashed lines mark the signal region of ω, the non-ω regions (box A, B, C) are used to estimate the $\pi^+\pi^-\pi^0\chi_{c1,2}$ events in the $\chi_{c1,2}$ signal regions.

at $\sqrt{s} = 4.416$ GeV and in the χ_{c1} signal region at $\sqrt{s} = 4.599$ GeV.

The main backgrounds are found to be $e^+e^- \to \pi^+\pi^-\pi^0\chi_{c1,2}$, where $\pi^+\pi^-\pi^0$ are of nonresonant origin. The $\pi^+\pi^-\pi^0\chi_{c1,2}$ background will produce a peak in the $\chi_{c1,2}$ signal region. The non-ω regions (box A, B, C), as shown in Fig. 1, are used to estimate the background. The number of $\pi^+\pi^-\pi^0\chi_{c1,2}$ events in the $\chi_{c1,2}$ signal regions can be calculated by $n_{1,2}^{bkg} = f \cdot (n_{A,B} - 0.5 n_C)$, where n_A, n_B, n_C are the numbers of events in boxes A, B, and C, and f is a normalization factor. To estimate the normalization factor f, we use the phase-space (PHSP) generator to simulate $\pi^+\pi^-\pi^0\chi_{c1,2}$ events at $\sqrt{s} = 4.416$ and 4.599 GeV.

Other possible backgrounds come from $e^+e^- \to \eta'J/\psi$ with $\eta' \to \gamma\omega$, $e^+e^- \to \pi^+\pi^-\psi'$ with $\psi' \to \pi^0\pi^0 J/\psi$ or $\gamma\chi_{c1,2}$, and $e^+e^- \to \pi^0\pi^0\psi'$ with $\psi' \to \pi^+\pi^- J/\psi$. All these backgrounds will not produce peaks in the signal regions, and their contribution is estimated to be negligible.

Figure 2 shows the $M(\gamma J/\psi)$ distributions at $\sqrt{s} = 4.416$ and 4.599 GeV for events in the J/ψ and ω signal region. Significant χ_{c2} signals at $\sqrt{s} = 4.416$ GeV and χ_{c1} signals at $\sqrt{s} = 4.599$ GeV are visible. Unbinned maximum likelihood fits are performed to measure the signal yields. The signal shapes are determined from signal MC samples. The shapes of the peaking background are determined by the $\pi^+\pi^-\pi^0\chi_{c1,2}$ MC sample, and the magnitudes are fixed at the expectation based on the non-ω region as mentioned above. The nonpeaking backgrounds are described with a constant. The fit results are shown in Fig. 2. For data at $\sqrt{s} = 4.416$ GeV, the $\omega\chi_{c1}$ signal yield is
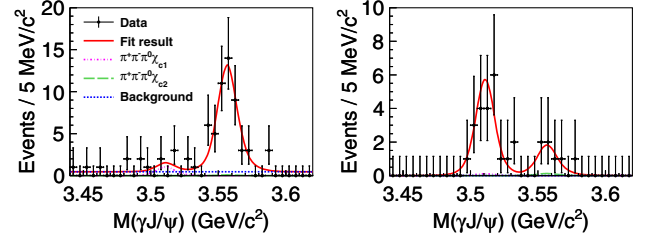

FIG. 2. Fits to the invariant mass $M(\gamma J/\psi)$ distributions for data at $\sqrt{s} = 4.416$ GeV (left) and 4.599 GeV (right). The red solid curves are the fit results. The magenta dashed-dotted curves and green long-dashed curves show the $\pi^+\pi^-\pi^0\chi_{c1}$ and $\pi^+\pi^-\pi^0\chi_{c2}$ peaking backgrounds, the blue dashed curves represent the flat background.

$0.0^{+3.7}_{-0.0}$, and the $\omega\chi_{c2}$ signal yield is 49.3 ± 7.5. The statistical significance of the χ_{c2} signal is 10.4σ by comparing the difference of log-likelihood values $[\Delta(\ln\mathcal{L}) = 54.0]$ with or without the χ_{c2} signal in the fit and taking into account the change of the number of degrees-of-freedom (Δndf $= 1$). For data at $\sqrt{s} = 4.599$ GeV, the $\omega\chi_{c1}$ signal yield is 21.1 ± 4.7 with a statistical significance of 7.4σ $[\Delta(\ln\mathcal{L}) = 27.5, \Delta$ndf $= 1]$, and the $\omega\chi_{c2}$ signal yield is $7.0^{+3.2}_{-2.5}$ with a statistical significance of 3.8σ $[\Delta(\ln\mathcal{L}) = 7.1, \Delta$ndf $= 1]$. The detailed information can be found in Table I.

Due to the limited integrated luminosity, the $\omega\chi_{c1,2}$ signals at the other energy points ($\sqrt{s} = 4.467$, 4.527, and 4.574 GeV) are not significant, and upper limits at the 90% C.L. are derived. The signal yields are obtained by counting events in the $\chi_{c1,2}$ signal regions and subtracting the backgrounds which are estimated from the $\chi_{c1,2}$ side-bands. The peaking backgrounds here are negligible. For the $\omega\chi_{c0}$ decay mode, signals are not significant at any of the energy points. We construct a likelihood function by assuming that the observed events follow a Poisson distribution and the background events follow a Gaussian distribution, where the signal yields are limited to be positive. From the likelihood distribution, the signal yields and uncertainties are determined.

The Born cross section is calculated with

$$\sigma^B(e^+e^- \to \omega\chi_{c1,2}) = \frac{N^{\text{sig}}}{\mathcal{L}(1+\delta)\frac{1}{|1-\Pi|^2}(\epsilon_e\mathcal{B}_e + \epsilon_\mu\mathcal{B}_\mu)\mathcal{B}_1},$$

(1)

where N^{sig} is the number of signal events, $\mathcal{L}$ is the integrated luminosity, $(1+\delta)$ is the radiative correction factor obtained from a quantum electrodynamics (QED) calculation [26,27] using the measured cross section as input and iterated until the results converge; $\frac{1}{|1-\Pi|^2}$ is the vacuum polarization factor which is taken from a QED calculation with an accuracy of 0.5% [28]; ϵ_e (ϵ_μ) is the

TABLE I. Results on $e^+e^- \to \omega\chi_{cJ}(J = 0, 1, 2)$. Shown in the table are the channels, the center-of-mass energy, the integrated luminosity $\mathcal{L}$, product of radiative correction factor, vacuum polarization factor, branching fraction and efficiency, $\mathcal{D} = (1 + \delta)\frac{1}{|1-\Pi|^2}(\epsilon_e\mathcal{B}_e + \epsilon_\mu\mathcal{B}_\mu)\mathcal{B}_1$ for $\omega\chi_{c1,2}$ and $\mathcal{D} = (1+\delta)\frac{1}{|1-\Pi|^2}(\epsilon_\pi\mathcal{B}(\chi_{c0}\to\pi^+\pi^-)+\epsilon_K\mathcal{B}(\chi_{c0}\to K^+K^-))\mathcal{B}(\omega\to\pi^+\pi^-\pi^0)\mathcal{B}(\pi^0\to\gamma\gamma)$ for $\omega\chi_{c0}$, number of observed events N^{obs}, number of estimated background events N^{bkg}, number of signal events N^{sig} determined as described in the text, and Born cross section σ^B (or upper limit at 90% C.L.) at each energy point. Here, the first errors are statistical, and the second systematic. N^{sig} for $\omega\chi_{c1,2}$ at $\sqrt{s} = 4.416$ and 4.599 GeV is taken from the fit. Dash means that the result is not applicable.

Channel	$\sqrt{s}$ (GeV)	$\mathcal{L}$ (pb^{-1})	$\mathcal{D}(\times 10^{-3})$	N^{obs}	N^{bkg}	N^{sig}	σ^B (pb)
$\omega\chi_{c0}$	4.416	1074	2.35	52	54.6 ± 9.4	$0.0^{+9.5}_{-0.0}$	< 7
	4.467	110	2.14	13	9.4 ± 1.7	$3.6^{+4.2}_{-3.6}$	< 49
	4.527	110	2.14	7	4.1 ± 1.3	$2.9^{+3.0}_{-2.6}$	< 37
	4.574	48	1.83	3	1.4 ± 0.7	$1.6^{+2.0}_{-1.6}$	< 65
	4.599	567	3.00	25	21.1 ± 3.1	$3.9^{+5.8}_{-3.9}$	< 9
$\omega\chi_{c1}$	4.416	1074	3.89	10	$6.3^{+2.7}_{-1.9}$	$0.0^{+3.7}_{-0.0}$	< 3
	4.467	110	3.72	3	$0.0^{+0.6}_{-0.0}$	$3.0^{+3.0}_{-1.6}$	< 18
	4.527	110	3.71	0	$0.0^{+0.6}_{-0.0}$	$0.0^{+1.3}_{-0.0}$	< 5
	4.574	48	3.77	3	$0.0^{+0.6}_{-0.0}$	$3.0^{+3.0}_{-1.6}$	< 39
	4.599	567	3.91	$\cdots$	$\cdots$	21.1 ± 4.7	$9.5 \pm 2.1 \pm 1.3$
$\omega\chi_{c2}$	4.416	1074	2.20	$\cdots$	$\cdots$	49.3 ± 7.5	$20.9 \pm 3.2 \pm 2.5$
	4.467	110	2.16	4	$0.0^{+0.6}_{-0.0}$	$4.0^{+3.2}_{-1.9}$	< 36
	4.527	110	2.18	0	$0.0^{+0.6}_{-0.0}$	$0.0^{+1.3}_{-0.0}$	< 9
	4.574	48	2.16	2	$0.0^{+0.6}_{-0.0}$	$2.0^{+2.7}_{-1.3}$	< 53
	4.599	567	2.30	7	$0.5^{+0.9}_{-0.4}$	$7.0^{+3.2}_{-2.5}$	< 11

global selection efficiency for the $e^+e^- \to \omega\chi_{c1,2}, \chi_{c1,2} \to \gamma J/\psi, J/\psi \to e^+e^-$ $(\mu^+\mu^-)$ decay mode, $\mathcal{B}_e$ $(\mathcal{B}_\mu)$ is the branching fraction $\mathcal{B}(J/\psi \to e^+e^-)$ $[\mathcal{B}(J/\psi \to \mu^+\mu^-)]$, $\mathcal{B}_1$ is the product branching fraction $\mathcal{B}(\chi_{c1,2}\to\gamma J/\psi)\times\mathcal{B}(\omega\to\pi^+\pi^-\pi^0)\times\mathcal{B}(\pi^0\to\gamma\gamma)$. The Born cross section (or its upper limit) at each energy point for $e^+e^- \to \omega\chi_{cJ}$ is listed in Table I.

For the energy points where the signals are not significant, the upper limits on the cross sections are provided. The upper limit is calculated by using a frequentist method with unbounded profile likelihood, which is implemented by the package TROLKE [29] in the ROOT framework. The number of the background events is assumed to follow a Poisson distribution, and the efficiency is assumed to have Gaussian uncertainties. In order to consider the systematic uncertainty in the upper limit calculation, we use the denominator in Eq. (1) as an effective efficiency as implemented in TROLKE.

The systematic uncertainties on the Born cross section measurement mainly originate from the detection efficiency, the radiative corrections, the fit procedure, the branching fractions, and the luminosity measurement.

The uncertainty in the tracking efficiency is 4.0% for both e^+e^- and $\mu^+\mu^-$ decay modes (1.0% per track) [19]. The uncertainty in photon reconstruction is 1.0% per photon, obtained by studying the $J/\psi \to \rho^0\pi^0$ decay [30].

In order to estimate the uncertainty caused by the angular distribution, the ω helicity angular distribution is set to $1 \pm \cos^2\theta_1$ (where θ_1 is the polar angle of ω in the e^+e^- rest frame with the z axis pointing in the electron beam direction) in the generator instead of the PHSP model, and the photon (from $\chi_{c1,2}$) helicity angular distribution is also set to $1 \pm \cos^2\theta_2$ (where θ_2 is the polar angle of the photon in the $\chi_{c1,2}$ rest frame, with the z axis pointing in the ω direction) in the generator instead of the PHSP model. The maximum change in the MC efficiencies is taken as the systematic uncertainty.

In the analysis, the helix parameters for simulated charged tracks have been corrected so that the MC simulation matches the momentum spectra of the data well [31]. The correction factors for π, e, and μ are obtained by using control samples $e^+e^- \to \pi^+\pi^-J/\psi, J/\psi \to e^+e^-$, and $\mu^+\mu^-$, respectively. The difference in MC efficiency between results obtained with and without the correction is taken as the systematic uncertainty.

The line shapes of $e^+e^- \to \omega\chi_{c1,2}$ will affect the radiative correction factor and the efficiency. The uncertainty is estimated by varying the line shapes of the cross section in the generator from the measured cross section to the $Y(4660)$ Breit-Wigner (BW) shape for $\omega\chi_{c1}$ and to the $\psi(4415)$ BW shape for $\omega\chi_{c2}$. The change in the final result between the two line shapes is taken as the uncertainty from the radiative correction factor.

TABLE II.   Relative systematic uncertainties for the luminosity, efficiency, line shape, fit procedure, and branching fractions (in units of %). The first value in brackets is for $\omega\chi_{c0}$, the second for $\omega\chi_{c1}$, and the third for $\omega\chi_{c2}$. Dash means that the result is not applicable.

Source/$\sqrt{s}$	4.416	4.467	4.527	4.574	4.599
Luminosity	1.0	1.0	1.0	1.0	1.0
Tracking	4.0	4.0	4.0	4.0	4.0
Photon	(2.0, 3.0, 3.0)	(2.0, 3.0, 3.0)	(2.0, 3.0, 3.0)	(2.0, 3.0, 3.0)	(2.0, 3.0, 3.0)
J/ψ mass window	($\cdots$, 1.6, 1.6)	($\cdots$, 1.6, 1.6)	($\cdots$, 1.6, 1.6)	($\cdots$, 1.6, 1.6)	($\cdots$, 1.6, 1.6)
Kinematic fit	(1.3, 2.0, 2.1)	(1.3, 1.9, 1.6)	(1.1, 2.0, 1.8)	(0.3, 2.0, 1.7)	(0.5, 2.3, 2.0)
Angular distribution	(2.5, 6.0, 6.1)	(3.2, 7.2, 8.3)	(2.5, 9.6, 8.0)	(3.5, 9.3, 10.1)	(1.7, 11.0, 10.3)
Line shape	(7.1, 1.2, 1.7)	(13.4, 1.0, 3.6)	(7.3, 0.5, 1.3)	(5.6, 0.9, 1.3)	(10.9, 1.0, 2.9)
Fit Range	($\cdots$, $\cdots$, 3.9)	$\cdots$	$\cdots$	$\cdots$	($\cdots$, 0.1, $\cdots$)
Flat background	($\cdots$, $\cdots$, 4.5)	$\cdots$	$\cdots$	$\cdots$	($\cdots$, 0.0, $\cdots$)
Peaking background	($\cdots$, $\cdots$, 4.1)	$\cdots$	$\cdots$	$\cdots$	($\cdots$, 1.9, $\cdots$)
Cross feed	(1.4, $\cdots$, $\cdots$)	(1.7, $\cdots$, $\cdots$)	(4.1, $\cdots$, $\cdots$)	(7.7, $\cdots$, $\cdots$)	(8.0, $\cdots$, $\cdots$)
$\mathcal{B}_e$, $\mathcal{B}_\mu$	($\cdots$, 0.6, 0.6)	($\cdots$, 0.6, 0.6)	($\cdots$, 0.6, 0.6)	($\cdots$, 0.6, 0.6)	($\cdots$, 0.6, 0.6)
$\mathcal{B}_1$	(3.8, 3.6, 3.7)	(3.8, 3.6, 3.7)	(3.8, 3.6, 3.7)	(3.8, 3.6, 3.7)	(3.8, 3.6, 3.7)
Sum	(9.8, 9.2, 11.8)	(15.2, 10.0, 11.3)	(10.6, 11.8, 10.6)	(11.4, 11.6, 12.3)	(14.9, 13.2, 12.7)

In the nominal fit, the fit range is taken from 3.44 to 3.62 GeV/c^2. The uncertainty from the fit range is obtained by varying the limits of the fit range by ± 0.025 GeV/c^2. The systematic uncertainty caused by the flat background shape is estimated by changing the background shape from a constant to a first-order polynomial. To estimate the uncertainty caused by the peaking background, we vary the number of the peaking background events by one standard deviation in the fit and cite the larger difference of the cross sections from the nominal values as the systematic uncertainty.

The luminosity is measured using Bhabha events with an uncertainty of 1.0% [24]. The branching fractions $\mathcal{B}_e$, $\mathcal{B}_\mu$, and $\mathcal{B}_1$ are taken from the world average [32], and their uncertainties are considered in the systematic uncertainty. The J/ψ mass window requirement has been studied in Ref. [33], and a 1.6% systematic uncertainty is assigned. The uncertainty due to the cross feed between the $\pi^+\pi^-$ and K^+K^- modes is estimated by using the signal MC samples.

Table II summarizes all systematic uncertainties of the processes $e^+e^- \to \omega\chi_{cJ}$, where the first values in brackets are for $\omega\chi_{c0}$, the second for $\omega\chi_{c1}$, and the third for $\omega\chi_{c2}$. The overall systematic uncertainties are obtained as the quadratic sum of all the sources of systematic uncertainties, assuming they are independent.

In Fig. 3, we compare the line shapes of the Born cross sections for $e^+e^- \to \omega\chi_{cJ}$, where the Born cross sections for $e^+e^- \to \omega\chi_{cJ}$ at $\sqrt{s} < 4.4$ GeV are from Ref. [19]. Enhancements can be seen in the line shapes; in the following, we try to fit line shapes. The cross section of $e^+e^- \to \omega\chi_{c0}$ with the addition of higher energy points is refitted with a phase-space modified BW function [19], and the fit results for the structure parameters are $\Gamma_{ee}\mathcal{B}(\omega\chi_{c0}) = (2.8 \pm 0.5 \pm 0.4)$ eV, $M = (4226 \pm 8 \pm 6)$ MeV/c^2, and $\Gamma_t = (39 \pm 12 \pm 2)$ MeV, which are almost unchanged. In the $e^+e^- \to \omega\chi_{c2}$ cross section, an enhancement is seen
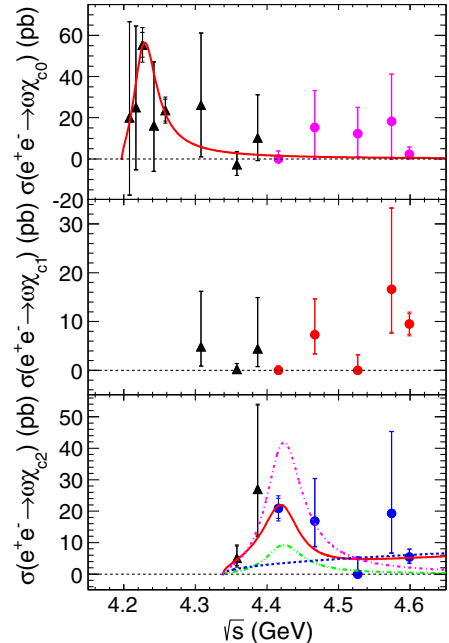

FIG. 3.   Measured Born cross section (center value) for $e^+e^- \to \omega\chi_{cJ}(J = 0, 1, 2)$ as a function of the center of mass energy. The top plot is for $e^+e^- \to \omega\chi_{c0}$, the middle plot for $e^+e^- \to \omega\chi_{c1}$, and the bottom plot for $e^+e^- \to \omega\chi_{c2}$, where the smaller errors are statistical only and the larger errors are the quadratic sum of the statistical and systematic errors. The triangle black points are from Ref. [19] and others are from this analysis. The $\sigma(e^+e^- \to \omega\chi_{c0})$ is fitted with a resonance(solid curve) in the top plot. $\sigma(e^+e^- \to \omega\chi_{c2})$ is fitted with the coherent sum of the $\psi(4415)$ BW function and a phase-space term. The solid curve shows the fit result, the blue dashed curve is the phase-space term, which is almost the same for the two solutions. The purple dash-dotted curve is the destructive solution and the green dash-double-dotted curve is the constructive one.

around 4.416 GeV, so we use a coherent sum of the $\psi(4415)$ BW function and a phase-space term

$$\sigma(\sqrt{s}) = \left| \frac{\sqrt{12\pi\Gamma_{ee}\mathcal{B}(\omega\chi_{c2})\Gamma_t}}{s - M^2 + iM\Gamma_t} \sqrt{\frac{\Phi(\sqrt{s})}{\Phi(M)}} e^{i\phi} + A\sqrt{\Phi(\sqrt{s})} \right|^2,$$
(2)

to fit the cross section, where M, Γ_t, Γ_{ee} are mass, total width, e^+e^- partial width for $\psi(4415)$, and are fixed to the known $\psi(4415)$ parameters [32], $\mathcal{B}(\omega\chi_{c2})$ is the branching fraction of $\psi(4415) \to \omega\chi_{c2}$, $\Phi(\sqrt{s}) = p/\sqrt{s}$ is the phase-space factor for an S-wave two-body system, where p is the ω momentum in the e^+e^- center-of-mass frame, ϕ is the phase angle, and A is the amplitude for the phase-space term. Two solutions are obtained with the same fit quality, the constructive solution is $\phi = 124° \pm 35°$, $\mathcal{B}(\omega\chi_{c2}) = (1.4 \pm 0.5) \times 10^{-3}$; the destructive one is $\phi = -105° \pm 15°$, $\mathcal{B}(\omega\chi_{c2}) = (6 \pm 1) \times 10^{-3}$. The goodness of fit is $\chi^2/\mathrm{ndf} = 4.6/4$.

In summary, using data samples collected at $\sqrt{s} > 4.4$ GeV, the processes $e^+e^- \to \omega\chi_{c1,2}$ are observed. With an integrated luminosity of 1074 pb^{-1} near $\sqrt{s} = 4.42$ GeV, a significant $\omega\chi_{c2}$ signal is seen, and the cross section is measured to be $(20.9 \pm 3.2 \pm 2.5)$ pb, where the first uncertainty is statistical and the second is systematic. Near $\sqrt{s} = 4.6$ GeV a clear $\omega\chi_{c1}$ signal is observed in 567 pb^{-1} of data, with a cross section of $(9.5 \pm 2.1 \pm 1.3)$ pb; evidence for an $\omega\chi_{c2}$ signal is found. The $\omega\chi_{c1,2}$ signals at other energies and the $\omega\chi_{c0}$ signals are not significant, the upper limits on the Born cross section at 90% C.L. are calculated. Interesting line shapes are observed for $\omega\chi_{cJ}$. There is an enhancement for $\omega\chi_{c2}$ around 4.42 GeV, which doesn't appear in the $\omega\chi_{c0,1}$ channels. A coherent sum of the $\psi(4415)$ BW function and a phase-space term can well describe the $\omega\chi_{c2}$ line shape, and the branching fraction $\mathcal{B}(\psi(4415) \to \omega\chi_{c2})$ is found to be in the order of 10^{-3}. The cross section of $e^+e^- \to \omega\chi_{c1}$ seems to be rising near 4.6 GeV. The $\omega\chi_{c0}$ is

refitted with the higher energy points included, and the fit results remain almost unchanged. The different line shapes observed for $\omega\chi_{cJ}$ might indicate that the production mechanism is different, and that nearby resonances [e.g., $\psi(4415)$] have different branching fractions to the $\omega\chi_{cJ}(J = 0, 1, 2)$ decay modes. Further studies based on more data samples at a higher energy will be helpful to clarify the nature of charmonium(like) states in this region.

[1] S. K. Choi *et al.* (Belle Collaboration), Phys. Rev. Lett. **91**, 262001 (2003).

[2] D. Acosta *et al.* (CDF Collaboration), Phys. Rev. Lett. **93**, 072001 (2004).

[3] B. Aubert *et al.* (*BABAR* Collaboration), Phys. Rev. Lett. **95**, 142001 (2005).

[4] T. E. Coan *et al.* (CLEO Collaboration), Phys. Rev. Lett. **96**, 162003 (2006).

[5] C. Z. Yuan *et al.* (Belle Collaboration), Phys. Rev. Lett. **99**, 182004 (2007).

[6] B. Aubert *et al.* (*BABAR* Collaboration), Phys. Rev. Lett. **98**, 212001 (2007).

[7] X. L. Wang *et al.* (Belle Collaboration), Phys. Rev. Lett. **99**, 142002 (2007).

[8] N. Brambilla, S. Eidelman, B. K. Heltsley, R. Vogt, G. T. Bodwin, E. Eichten, A. D. Frawley, and A. B. Meyer *et al.*, Eur. Phys. J. C **71**, 1534 (2011).

[9] M. Ablikim *et al.* (BESIII Collaboration), Phys. Rev. Lett. **110**, 252001 (2013).

[10] Z. Q. Liu *et al.* (Belle Collaboration), Phys. Rev. Lett. **110**, 252002 (2013).

[11] T. Xiao, S. Dobbs, A. Tomaradze, and K. K. Seth, Phys. Lett. B **727**, 366 (2013).

[12] M. Ablikim *et al.* (BESIII Collaboration), Phys. Rev. Lett. **115**, 112003 (2015).

[13] M. Ablikim *et al.* (BESIII Collaboration), Phys. Rev. Lett. **112**, 022001 (2014).

[14] M. Ablikim *et al.* (BESIII Collaboration), Phys. Rev. Lett. **115**, 222002 (2015).

[15] M. Ablikim *et al.* (BESIII Collaboration), Phys. Rev. Lett. **111**, 242001 (2013).

[16] M. Ablikim *et al.* (BESIII Collaboration), Phys. Rev. Lett. **113**, 212002 (2014).

[17] M. Ablikim *et al.* (BESIII Collaboration), Phys. Rev. Lett. **112**, 132001 (2014).

[18] M. Ablikim *et al.* (BESIII Collaboration), Phys. Rev. Lett. **115**, 182002 (2015).

[19] M. Ablikim *et al.* (BESIII Collaboration), Phys. Rev. Lett. **114**, 092003 (2015).

[20] L. Y. Dai, M. Shi, G. Y. Tang, and H. Q. Zheng, Phys. Rev. D **92**, 014020 (2015).

[21] D. Y. Chen, X. Liu, and T. Matsuki, Phys. Rev. D **91**, 094023 (2015).

[22] X. Li and M. B. Voloshin, Phys. Rev. D **91**, 034004 (2015).

[23] M. Ablikim *et al.* (BESIII Collaboration), Nucl. Instrum. Methods Phys. Res., Sect. A **614**, 345 (2010).

[24] M. Ablikim *et al.* (BESIII Collaboration), Chin. Phys. C **39**, 093001 (2015).

[25] M. Ablikim *et al.* (BESIII Collaboration), arXiv:1510.08654.

[26] E. A. Kuraev and V. S. Fadin, Sov. J. Nucl. Phys. **41**, 466 (1985).

[27] S. Jadach, B. F. L. Ward, and Z. Was, Comput. Phys. Commun. **130**, 260 (2000); Phys. Rev. D **63**, 113009 (2001).

[28] S. Actis *et al.* (Working Group on Radiative Corrections and Monte Carlo Generators for Low Energies Collaboration), Eur. Phys. J. C **66**, 585 (2010).

[29] W. A. Rolke, A. M. Lopez, and J. Conrad, Nucl. Instrum. Methods Phys. Res., Sect. A **551**, 493 (2005).

[30] M. Ablikim *et al.* (BESIII Collaboration), Phys. Rev. D **81**, 052005 (2010).

[31] M. Ablikim *et al.* (BESIII Collaboration), Phys. Rev. D **87**, 012002 (2013).

[32] K. A. Olive *et al.* (Particle Data Group), Chin. Phys. C **38**, 090001 (2014).

[33] M. Ablikim *et al.* (BESIII Collaboration), Phys. Rev. Lett. **112**, 092001 (2014).